ACS Biomaterials SCIENCE & ENGINEERING

pubs.acs.org/journal/abseba

Article

Electrostatic Assembly of Multiarm PEG-Based Hydrogels as Extracellular Matrix Mimics: Cell Response in the Presence and Absence of RGD Cell Adhesive Ligands

Panthipa Suwannakot, Stephanie Nemec, Newton Gil Peres, Eric Y. Du, Kristopher A. Kilian, Katharina Gaus, Maria Kavallaris, and J. Justin Gooding*

Cite This: https://doi.org/10.1021/acsbiomaterials.2c01252

Read Online

ACCESS | Metrics & More | Article Recommendations | Supporting Information

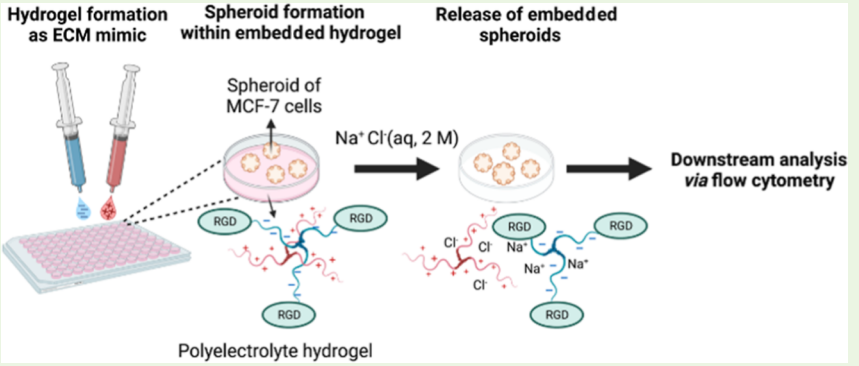

ABSTRACT: Synthetic hydrogels have been used widely as extracellular matrix (ECM) mimics due to the ability to control and mimic physical and biochemical cues observed in natural ECM proteins such as collagen, laminin, and fibronectin. Most synthetic hydrogels are formed *via* covalent bonding resulting in slow gelation which is incompatible with drop-on-demand 3D bioprinting of cells and injectable hydrogels for therapeutic delivery. Herein, we developed an electrostatically crosslinked PEG-based hydrogel system for creating high-throughput 3D in vitro models using synthetic hydrogels to mimic the ECM cancer environment. A 3-arm PEG-based polymer backbone was first modified with either permanent cationic charged moieties (2-(methacryloyloxy)ethyl trimethylammonium) or permanent anionic charged moieties (3-sulfopropyl methacrylate potassium salt). The resulting charged polymers can be conjugated further with various amounts of cell adhesive RGD motifs (0, 25, 75, and 98%) to study the influences of RGD motifs on breast cancer (MCF-7) spheroid formation. Formation, stability, and mechanical properties of hydrogels were tested with, and without, RGD to evaluate the cellular response to material parameters in a 3D environment. The hydrogels can be degraded in the presence of salts at room temperature by breaking the interaction of oppositely charged polymer chains. MCF-7 cells could be released with high viability through brief exposure to NaCl solution. Flow cytometry characterization demonstrated that embedded MCF-7 cells proliferate better in a softer (60 Pa) 3D hydrogel environment compared to those that are stiffer (1160 Pa). As the stiffness increases, the RGD motif plays a role in promoting cell proliferation in the stiffer hydrogel. Flow cytometry characterization demonstrated that embedded MCF-7 cells proliferate better in a softer (60 Pa) 3D hydrogel environment compared to those that are stiffer (1160 Pa). As the stiffness increases, the RGD motif plays a role in promoting cell proliferation in the stiffer hydrogel. Additionally, cell viability was not impacted by the tested hydrogel stiffness range between 60 to 1160 Pa. Taken together, this PEG-based tuneable hydrogel system shows great promise as a 3D ECM mimic of cancer extracellular environments with controllable biophysical and biochemical properties. The ease of gelation and dissolution through salt concentration provides a way to quickly harvest cells for further analysis at any given time of interest without compromising cell viability.

KEYWORDS: *RGD motif, stiffness, polyelectrolyte hydrogel, gel dissociation and release of breast cancer spheroids*

1. INTRODUCTION

There is a global effort to develop three-dimensional (3D) in vitro cell models which have been shown to reflect the cellular responses in *vivo* better than 2D cell cultures.[1−3] A crucial part of 3D cell cultures is the employed extracellular matrix (ECM). Hydrogels of synthetic polymers are often used as ECM mimics.[4,5] This is because such synthetic hydrogels have many

Received: October 23, 2022
Accepted: February 14, 2023

characteristics in common with ECM biopolymers such as gelatin, collagen, and fibronectin, with the added advantage that their mechanical and chemical properties are tuneable.[6,7] Frequently, the synthetic ECM mimics use poly(ethylene glycol) (PEG) as a structural element because of their low amount of interaction with cells such that the cell responses can be controlled by conjugating bioactive molecules, such as cell-adhesive ligands or cell cleavable moieties.[8,9] For example, the high degree of control over the chemistry of the polymer chains allows one to develop ECM mimics where cell adhesion, cell remodeling, and stiffness can be modulated.[10−12]

The gelation process of polymeric hydrogels from solution to a hydrogel state involves crosslinking of the polymer chains that are the hydrogel precursors *via* either chemical (covalent) or physical (non-covalent) bonds to form a 3D hydrogel network.[13] Most biopolymer hydrogels rely on physical crosslinking to stabilize the material, while most synthetic hydrogels are crosslinked chemically.[14,15] Apart from the control over the polymer properties, the power of the chemical gelation is the robustness of the final polymer but at the cost of gelation time (typically on the order of minutes or longer).[12,16,17] Rapid gelation is needed in applications such as 3D bioprinting of cells[18,19] and injectable hydrogels for therapeutic delivery.[20] Recently, Nguyen et al. reported a physically crosslinked synthetic hydrogel by developing a diblock (AB-) copolymer hydrogel system with PEG forming the main polymer backbone with at either end of the polymer chain a permanent anionic or permanent cationic charged moiety.[21] Equimolar mixing of the positively charged polymers with the negatively charged polymers resulted in almost instantaneous gelation as observed for biopolymer ECM mimics.

This initial proof of concept paper explored the tunability of the PEG-based polymer in terms of physical properties and showed that the system was compatible with MCF-7 breast cancer cells. In addition to rapid gelation, another desirable feature of 3D ECM mimics is the ability to harvest the cell population quickly and mildly for analysis which is a critical aspect for the future of high content bioassays. Currently, most chemically crosslinked PEG-based hydrogels are degraded via sophisticated designs such as functionalizing with cleavable crosslinks, e.g., matrix metalloproteinases (MMPs),[22,23] conjugating photolabile moieties[24,25] or hydrolyzing the bond.[26,27] The degradation rate is often slow and unpredictable which can be problematic as the hydrogel scaffold can significantly affect osteogenesis, chondrogenesis, neurogenesis, and ECM cell deposition.[28] For example, rapid scaffold degradation can dramatically change hydrogel porosity, preventing proper ECM build-up as ECM molecules tend to diffuse away. In contrast, slow degradation can prevent the proper distribution of deposited ECM throughout the hydrogel.[29,30] As such, it is important to match scaffold degradation to endogenous ECM production by allowing degradation to occur at a specific time point of interest for a particular study. The purpose of the study herein was to explore this polyelectrolyte di-block copolymer hydrogel system in detail. This included understanding the stability of the hydrogels in the cell culture medium, showing how to tune the presentation of chemical cues on cell biology through the conjugation of RGD ligands to the cells, and how to dissociate the hydrogels to recover cells for downstream applications.

2. EXPERIMENTAL SECTION

2.1. Materials. 4-Cyano-4-(phenylcarbonothioylthio)pentanoic acid *N*-succinimidyl ester (>97%, Sigma-Aldrich), 3-arm PEG amine hydrochloride salt (3-arm PEG-NH_2·HCl, >98%, M_n = 15 kDa, JemKem Technology), 3-sulfopropyl methacrylate potassium salt (98%, Sigma-Aldrich), 2-(methylacryloyloxy)ethyl trimethylammonium (75%, Sigma-Aldrich), 4,4′-azobis(4-cyanovaleric acid) (ACVA, Sigma-Aldrich), 6-maleimidohexanoic acid *N*-hydroxysuccinimide ester (98% HPLC, Chem-Impex), tris(2-carboxyethyl)phosphine (TCEP, 99% assay by titration, Chem-Impex), sodium chloride, calcium chloride, dimethylformamide (HPLC grade, Chem-Supply Pty Ltd. Australia), diethyl ether (VWR International, Pty Ltd.), PBS (pH = 7.4), Dulbecco's phosphate-buffered saline (no calcium, no magnesium, DPBS, Life Technologies, Australia), Dulbecco's modified Eagle medium (DMEM, Thermo Fisher Scientific, USA) fetal bovine serum (FBS, Thermo Fisher Scientific, USA), and dialysis tubing cellulose membrane (MWCO 14,000, Sigma-Aldrich) were used as received. Deuterium oxide (D_2O, 99.9%, Cambridge Isotope Laboratories Inc.) was used as received as an NMR solvent. All solvents used for synthesis and purification were of analytical grade. Milli-Q water (18 MΩ × cm) was used for all experiments unless stated otherwise.

2.2. Synthesis. *2.2.1. Synthesis, Purification, and Characterization of Polyelectrolyte 3-Arm PEG-Based Polymers.* The synthesis of polyelectrolyte 3-arm PEG-based polymers involves a two-step process: first, by making the 3-arm PEG MacroRAFT agent and then attaching the charged monomer onto the 3-arm PEG MacroRAFT agent.

2.2.1.1. Synthetic Procedure of 3-Arm PEG MacroRAFT Agent. The 3-arm PEG MacroRAFT agent containing PEG attached with three CPADB end groups was synthesized by NHS coupling according to Nguyen et al. (Figure S12).[21] In a typical synthesis of 3-arm PEG MacroRAFT agent, 3-arm PEG NH_2·HCl (MW = 15 kDa, 5.065 g, 0.333 mmol) was dissolved fully in PBS (pH = 7.4, 30 mL) and the CPADB succinimidyl ester (0.452 g, 1.2 mmol) was prepared separately and dissolved in DMF (65 mL). The two solutions were mixed to give a clear pink mixture, and it was stirred at room temperature for 24 h. The mixture was then precipitated with diethyl ether and dried under a high-pressure vacuum for overnight to yield a pink solid (5.667 g). ^{1}H NMR (400 MHz, D_2O, Figure S13): δ (ppm) 1.75 (s, 3H, C**H**$_3$), 2.70 (s, 2H, C**H**$_2$−C═O), 2.81 (s, 2H, CC**H**$_2$), 3.63 (s, 4*n*H, (C**H**$_2$C**H**$_2$−O)$_n$), 7.45 (t, 2H, ArH), 7.70 (t, 1H, ArH), 8.70 (d, 2H, Ar**H**-C═S), where *n* is the degree of polymerization.

2.2.1.2. RAFT Polymerization of Negatively Charged Monomer (SPMA) Using 3-Arm PEG MacroRAFT Agent. The 3-arm PEG MacroRAFT agent was coupled with 3-sulfopropyl methacrylate potassium salt monomer *via* RAFT polymerization to yield 3-arm PEG-*block*-PSPMA polymers according to Nguyen et al. (Figure S14).[21] In a smaller scale reaction, RAFT agent (1 equiv, 3.157 × 10^{-5} mol, 0.501 g), monomer (252 equiv, 7.955 × 10^{-3} mol, g), and ACVA initiator (0.2 equiv, 6.314 × 10^{-6} mol, 1.770 mL) were dissolved in Milli-Q water (14.14 mL) and the overall concentration of the polymer solution was kept constant at 0.5 M. The polymer solution was sonicated until the solution was clear and homogenous. The solution was then purged with Ar for 30 min, placed in a preheated oil bath at 70 °C, and stirred for 5 h. After that, the polymer solution was stopped and placed in an ice bath for 30 min to stop the polymerization and terminate the polymer chains. A small amount of sample was withdrawn, and NMR was performed to determine the polymerization conversion rate (90−95%). The polymer solution was then dialyzed against Milli-Q water using a 14 kDa cutoff dialysis tube for 2 days at room temperature, consistently changing the water once in the morning, noon, and afternoon to remove unreacted reagents. The polymer solution was then frozen at −80 °C and freeze-dried to yield an orange fluffy solid (1.960 g), which was then kept at room temperature until further use. ^{1}H NMR (400 MHz, D_2O, Figure S15): δ (ppm) 0.70−1.10 (m, 2*n*H, C**H**$_2$ of the main chain), 1.80−2.10 (m, 2*n*H, C**H**$_3$ of the main chain), 3.03 (t, 2*n*H, S−C**H**$_2$), 3.70 (s, 4*n*H,

https://doi.org/10.1021/acsbiomaterials.2c01252
ACS Biomater. Sci. Eng. XXXX, XXX, XXX−XXX

($CH_2CH_2O)_n$), 3.75−3.95 (br, s, $N^+(CH_3)_3$), 4.16 (br s, COO−CH_2), where n is the degree of polymerization.

2.2.1.3. RAFT Polymerization of Positively Charged Monomer (MAETMA) Using 3-Arm PEG MacroRAFT Agent. According to Nguyen et al., the 3-arm PEG MacroRAFT agent was coupled with 2-(methylacryloyloxy)ethyl trimethylammonium monomer *via* RAFT polymerization to yield PEG-*block*-PMAETMA polymers.[21] (Figure S14). In a small-scale reaction, RAFT agent (1 equiv, 3.156×10^{-5} mol, 0.500 g), monomer (350 equiv, 1.2×10^{-3} mol, 2.29 mL), and ACVA initiator (0.2 equiv, 6.313×10^{-6} mol, 1.770 mL) were dissolved in Milli-Q water (19.715 mL) and the overall concentration of the polymer solution was kept constant at 0.5 M. The polymer solution was sonicated until the pink solution turned clear and homogenous. The solution was then purged with Ar for 30 min, placed in a preheated oil bath at 70 °C, and stirred for 18 h. After that, the polymer solution was stopped and placed in an ice bath for 30 min to stop the polymerization and terminate the polymer chains. A small amount of sample was withdrawn, and NMR was performed to determine the polymerization conversion rate (90−95%). Molar equivalents of monomer units can be adjusted to achieve other chain lengths. Batch-to-batch variability was minimized by only using batches with similar stiffness. The polymer solution was then dialyzed against Milli-Q water for 2 days (molecular weight cutoff of 14 kDa), consistently changing the water in the morning, noon, and afternoon before freeze-drying to yield an orange fluffy solid (1.850 g). ^{1}H NMR (400 MHz, D_2O, Figure S16): δ (ppm) 0.72−1.49 (m, 2nH, CH_2 of the main chain), 1.88−2.35 (m, 3nH, CH_3 of the main chain), 3.30 (s, 3H, CH_3), 3.72 (s, 4nH, ($CH_2CH_2O)_n$), 3.90 (br s, N−CH_2) and 4.64 (br s, COO−CH_2), where n is the degree of polymerization.

2.2.2. Synthesis, Purification, and Characterization of Anionic 3-Arm PEG-Based Polymers Conjugated RGD Motifs. The bioconjugation of RGD was achieved in a "one-pot" reaction in which the reaction occurs in two reaction steps. In the first step, 3-arm PEG-based cationic polymers (1 equiv, 10.0 g) were dissolved in $NaBH_4$(aq) (0.5 M, 200 mL). The mixture was stirred at room temperature for 2 h, followed by the addition of tris(2-carboxyethyl)-phosphine (TCEP) (200 equiv, 3440 mg) in Milli-Q water (5 mL). The mixture was stirred overnight at room temperature to reduce the trithiocarbonate functionality of the polymer RAFT end group to 3-arm PEG-based polymeric thiols. In parallel, the mixture of 6-maleimidohexano-RGD was prepared by mixing a solution of RGD solid (12 equiv, 1068 mg) in $NaHCO_3$ (50 mM, 30 mL) and 6-maleimidohexanic acid *N*-hydroxy succinimide ester (6 equiv, 600 mg) in $NaHCO_3$ (50 mM, 60 mL) overnight at room temperature to yield 6-maleimidohexano-RGD compound (86.7%). In the second step, a mixture of the 6-maleimidohexano-RGD was mixed with the 3-arm cationic polymeric thiols and stirred overnight at room temperature. The resulting mixture was dialyzed against Milli-Q water to remove any unconjugated residues for a day using a molecular weight cutoff of 14 kDa with consistently changing the water in the morning, noon, and afternoon before freeze-drying to yield RGD-modified 3-arm PEG-based polymers (9.890 g, 98.9%). IR (FT-IR, ATR iD7 Diamond): 1550 cm^{-1} (N−H bending), 1660 cm^{-1} (C═O stretching), 1730 cm^{-1} (C═O stretching).

2.3. Preparation of Polyelectrolyte 3-Arm PEG-Based Hydrogels. The charged polymer solids were prepared to a desirable concentration (% w/v) by balancing the charges (1:1 charge ratio) on both cationic and anionic polymer chains. The charges on polymers can be calculated according to the number of monomer repeating units (RUs), assuming that one monomer RU equals one charge on the polymer chains. Each weighed polymer was dissolved separately in a specific solvent of interest. For example, a 20% w/v polymer solution of polymers with 150 RUs was prepared by weighing 250.21 mg of cationic polymers and 249.79 mg of anionic polymers and dissolved separately in 1 mL. Finally, an equal volume of cationic and anionic polymer solutions was then mixed to form a polyelectrolyte hydrogel. Full detail on how to prepare polymer solution can be found in the Supporting Information.

2.4. Characterization of Synthesized Polymers Using ^{1}H NMR. ^{1}H NMR spectra were analyzed on a Bruker ADVANCE III HD spectrometer (400 MHz). Deuterium oxide (D_2O) was used as received as a NMR solvent. Chemical shifts (symbol) were reported in parts per million (ppm), relative to the residual solvent peak. The residual proton signal of D_2O was used as an internal standard (sigma H = 4.79 for D_2O). The NMR spectra were processed using the Bruker TOPSPIN 3.0 software. Multiplicities are assigned as singlet (s), doublet (d), doublet of doublet (dd), triplet (t), quartet (q), multiplet (m), and broad (br). Percentage conversion was determined as follows: % conversion = 100 × (integral polymer peak)/(integral monomer peak + integral polymer peak) of crude ^{1}H NMR. The theoretical molecular weights (M_n) of the polymers were calculated using eq 1

$$M_{n,theo} = \frac{[Monomer]_0}{[RAFT]_0} \times M.\,W._{\cdot monomer} \times \% \text{ conversion} \times M.\,W._{\cdot RAFT} \quad (1)$$

Equation 1: calculation of theoretical molecular weight ($M_{n,theo}$) of the synthesized polymers, where $[monomer]_0$ is the initial concentration of monomer, $[RAFT]_0$ is the initial RAFT concentration, $M.W._{\cdot monomer}$ is the molecular weight of the monomer, and $M.W._{\cdot RAFT}$ is the molecular weight of the RAFT agent.

2.5. Rheological Measurements. Rheological experiments on all hydrogels were performed using an Anton Paar MCR302 rheometer equipped with a parallel-plate geometry of 25 mm diameter and RheoCompass software. Rheological measurements were conducted using a solvent trap to minimize evaporation of the hydrogels. The measuring plate was lowered to a fixed gap height of 1 mm. The cationic and anionic polymer solids were prepared by dissolving separately in a solvent of interest [Milli-Q water, PBS, DMEM buffers, NaCl (aq) and $CaCl_2$ (aq)] at a 1:1 monomer charge ratio. The resulting cationic polymer solution (270 μL) and anionic polymer solution (270 μL) were loaded and mixed on the rheometer plate using a pipette tip to ensure complete gelation. The measurements were then performed with the oscillatory time sweep for 60 min to monitor the stability and gelation behavior at a fixed frequency of 1 Hz and 0.1% strain, followed by a frequency sweep (0.01−10 Hz) at 0.1% strain to confirm the expected gel viscoelasticity, and finally, two strain sweeps (0.1−100%) were conducted at a fixed frequency of 1 Hz. Two temperatures (25 and 37 °C) were used in all experiments unless mentioned otherwise. The results were then plotted using Origin 2018 where the data presented are an average of three individual repeats.

2.6. Mesh Size Calculation. Mesh size was calculated using the Flory−Rehner equation (eq 2) as previously described in literature. Briefly, swelling ratio was calculated for relaxed gels (Q_{mr}) and swollen gels (Q_m). The wet weight and dry weight of each sample was obtained and applied to the following formula

$$\text{mass swelling ratio} = Q_{m(r)} = \frac{m_{wet} - m_{lyophilised}}{m_{lyophilised}} \quad (2)$$

Volumetric (Q_{vr}) and equilibrium (Q_v) swelling ratios were then calculated using the following equation (eq 3), where polymer density (r_p) was taken as 1.125 g/cm^3 and solvent density (r_s) was taken as 1.011 for DMEM.

$$Q_{v(r)} = 1 + \frac{\rho_p}{\rho_s}(Q_{m(r)} - 1) \quad (3)$$

Relaxed polymer volume fraction (υ_{2r}) wand equilibrium polymer volume fraction (υ_{2s}) were calculated using the following equation (eq 4)

$$\upsilon = \frac{1}{Q_v} \quad (4)$$

The Flory−Rehner equation was then applied to calculate the molecular weight between crosslinks (M_c), where M_c is the average molecular weight of the polymer prior to crosslinking, $\bar{\upsilon}$ is the specific volume of the polymer (taken as 0.93 for PEG), V_1 was the molar

https://doi.org/10.1021/acsbiomaterials.2c01252
ACS Biomater. Sci. Eng. XXXX, XXX, XXX−XXX

volume of the solvent (18 mL/mol for water), and X_1 is the polymer−solvent interaction (0.426 for PEG in water) to give eq 5.

$$\frac{1}{M_c} = \frac{2}{M_n} - \frac{\frac{\overline{v}}{V_1}[\ln(1-\upsilon_{2s}) + \upsilon_{2s} + X_1\upsilon_{2s}^2]}{\upsilon_{2r}\left[\left(\frac{\upsilon_{2s}}{\upsilon_{2r}}\right)^{1/3} - \frac{1}{2}\left(\frac{\upsilon_{2s}}{\upsilon_{2r}}\right)\right]} \quad (5)$$

Lastly, mesh size (ξ) was calculated using the below equation, where M_r is the molecular weight of the RU, l is the bond length along the polymer backbone (0.15 nm for PEG), and C_n is the Flory characteristic ratio (4 for PEG) as in (eq 6).

$$\xi = \upsilon_{2s}^{-1/3} l \sqrt{\frac{2C_n M_c}{M_r}} \quad (6)$$

2.7. Cell Culture. *2.7.1. Breast Cancer Cells.* Frozen human immortalized breast cancer cells (MCF-7, ATCC) were harvested by thawing in 37 °C water and resuspended in pre-warmed high glucose DMEM culture medium (4.5 g/L D-glucose) supplemented with 10% v/v FBS (10 mL) and 1% v/v penicillin/streptomycin. The suspended cells were centrifuged (500*g*) for 5 min, and the supernatant was decanted to remove dimethyl sulfoxide (DMSO). The cell pellet was resuspended in DMEM media and transferred into a tissue culture flask. Cells were cultured in DMEM culture media and incubated in a 5% CO_2 atmosphere at 37 °C. The cell culture media was changed every 2−3 days, and the cells were passaged twice a week at 80−90% confluency, 2−3 times per week, between passages 10−25. DMEM culture media was removed, and the cells were washed with DPBS (1 × 10 mL), followed by the addition of trypsin (0.25% w/v, 3 mL) and incubation in a 5% CO_2 atmosphere at 37 °C for 3 min to detach the cells from the surface of the tissue culture flask. The suspended cell solution was dispersed in DMEM media (6 mL) and then centrifuged (500*g*) for 3 min. The DMEM media and trypsin solution were aspirated, followed by resuspension in DMEM media (10 mL). DMEM media (9 mL) were added to a new tissue culture flask before adding the cell suspension (1 mL) to create a new passage which was then incubated in a 5% CO_2 atmosphere at 37 °C for 2−3 days or until confluence was reached. The remaining cell suspension was used for subsequent cell experiments. All procedures were done under sterile conditions of physical containment level 2 (PC2).

2.7.2. Preparation of Samples. All chemicals and synthesized polymers were prepared in the non-sterile laboratory before proceeding to cell work where they were sterilized by filtering through a 0.22 μm syringe filter. The sample was prepared by dissolving polymers in DMEM medium culture according to the desired polymer concentration and then sterilized by filtering through a 0.22 μm syringe filter before adding to the cell pellet based on the desired cell density. The samples were prepared fresh and used within a day.

2.7.3. 3D Cell Encapsulation Viability Study. Breast cancer MCF-7 cells were detached from the flask using 0.25% w/v trypsin and counted with trypan blue solution (0.4% w/v, Gibco, USA). The trypsinized cells were then centrifuged (500*g* for 5 min), resuspended in warmed culture media, and counted using a hemocytometer to determine initial cell concentration. To obtain the desired cell concentration for the experiments, cells were taken from the initial cell concentration, centrifuged, and re-suspendered in 3-arm cationic PEG-based ink in DMEM culture media at the desired polymer concentration. Cell suspension in the cationic ink (25 μL) was pipetted onto a 96-well plate, followed by the addition of the anionic polymer ink (25 μL) dissolved in DMEM to form a hydrogel with a volume of 50 μL by quickly mixing the polymer components gently with a pipette tip. DMEM culture media (200 μL) was added to each well and incubated in a 5% CO_2 atmosphere at 37 °C, and the media was changed every two days.

2.7.4. Viability of MCF-7 Cells When Exposing to NaCl Solutions. MCF-7 cells were seeded (20,000 cells) in triplicates on a 96-well plate and were cultured in standard DMEM, supplemented with 10% v/v FBS and 1% v/v penicillin/streptomycin in a 5% CO_2 atmosphere at 37 °C for 48 h. All solutions were sterilized by filtering through a 0.22 μm pore syringe filter. Various concentrations of NaCl solution (100 μL) were added to each well and incubated for 5 min. The saline solution was carefully removed before adding a fresh DMEM with alamarBlue reagent (10% v/v) and further incubated at 37 °C for 2 h. The fluorescence intensity was measured using the Tecan Infinite 200 Pro Multimode Microplate Reader with an excitation wavelength of 540 nm and an emission wavelength of 590 nm. The mean absorbance values ± SD for each concentration of polymer components and hydrogels were determined, analyzed, and plotted using Origin 2020.

2.8. Imaging. *2.8.1. Brightfield.* An inverted brightfield microscope (Olympus) was used to capture images under 4× and 10× objectives every 1−2 days for the 7−14 day hydrogel embedded culture time. The morphology of spheroids was observed and recorded using a brightfield microscope. All images were processed using ImageJ 1.50 (National Institutes of Health, USA) which were then used to estimate the diameter of spheroids.

2.8.2. LIVE/DEAD. LIVE/DEAD staining was used to examine the viability of cells encapsulated within a hydrogel. The culture medium was removed, and the hydrogels were washed with DPBS (2 × 100 μL). A mixture of calcein AM (2 μM) and ethidium homodimer-l (4 μM) (ThermoFisher, USA) in DPBS (100 μL) was added to each well to stain the live and dead cells, respectively, and incubated for 20 min to allow the stain to diffuse into the hydrogels, followed by two DPBS washes with 10 min incubation before imaging. A confocal fluorescence microscope observed stained cells encapsulated within the hydrogels. The samples were imaged using a Zeiss LSM 800 confocal microscope at the Katharina Gaus Imaging Facility of the University of New South Wales, Sydney, Australia. A 10× objective with a 2100 μm working distance was used. LIVE/DEAD stain was recorded with a quad-band filter with an excitation of 350 and 494 nm and emission of 617 and 514 nm for Ethidium homodimer-1 and calcein, respectively.

2.8.3. Immunofluorescence Staining and Tissue Clearing. The samples were fixed in 4% w/v paraformaldehyde (Chem-Supply) overnight at room temperature, followed by washing with DPBS twice. Samples were permeabilized with 0.1% Triton X-100 (Fisher, USA) in DPBS for 30 min and blocked with 1% bovine serum albumin (BSA, Sigma, USA). Primary antibodies were used to label collagen I (rabbit polyclonal, 1:300, ab34710 Abcam, USA) hydrogel samples overnight at room temperature. The secondary antibody staining was performed with goat anti-rabbit IgG (H + L), Alexa Fluor 555 (1:200, ThermoFisher, USA) in 1% BSA solution in DPBS with Hoechst 33342 (1:300, ThermoFisher, USA), and 488-Phalloidin (1:300, Sigma, USA). The samples were washed with DPBS before adding the Cubic 2 clearing solution for 2−5 days. Cubic clearing solution 2 was prepared by mixing 50% w/w sucrose (Sigma-Aldrich, 584173), 25% w/w urea, and 10% w/w triethanolamine (Sigma-Aldrich, 90278−100 mL) with Milli-Q water at 55 °C. Samples remained in Cubic clearing solution 2 minimally overnight, before imaging. The samples were imaged using a Zeiss LSM 800 confocal microscope at the Katharina Gaus Imaging Facility of the University of New South Wales, Sydney, Australia. A 10× objective with a 2100 μm working distance was used. Immunostaining images were recorded with a quad-band filter with an excitation window of 353, 493, and 653 nm and an emission range of 465, 517, and 668 nm for Hoechst, 488-Phalloidin, and 555-Col I, respectively. The images were captured with a Zeiss Axiocam 305 monochrome camera, recorded with the Zen Blue software (Zeiss, Australia) and processed with ImageJ 1.49 (National Institutes of Health, USA).

2.8.4. Releasing Cells from Hydrogels Using 2 M NaCl Solution. To release the cells or spheroids from the hydrogel, 2 M NaCl solution was used as gel dissolution which was prepared from an equal volume of 4 M NaCl and DMEM culture medium supplemented with 10% v/v FBS (10 mL) and 1% v/v penicillin/streptomycin. The media was removed from each well, and 2 M NaCl solution (100 μL) was added to each well to dissociate the hydrogels with gentle pipetting for a maximum of 5 min.

2.8.5. Flow Cytometry. MCF-7 breast cancer cells were stained with CellTrace Violet (CTV—stains cytoplasm) and washed twice

https://doi.org/10.1021/acsbiomaterials.2c01252
ACS Biomater. Sci. Eng. XXXX, XXX, XXX−XXX

Scheme 1. Process of Forming Polyelectrolyte Hydrogel *via* Electrostatic Crosslink Interaction and Bioconjugation Pathway of Polyelectrolyte 3-Arm PEG-Based Polymers[a]

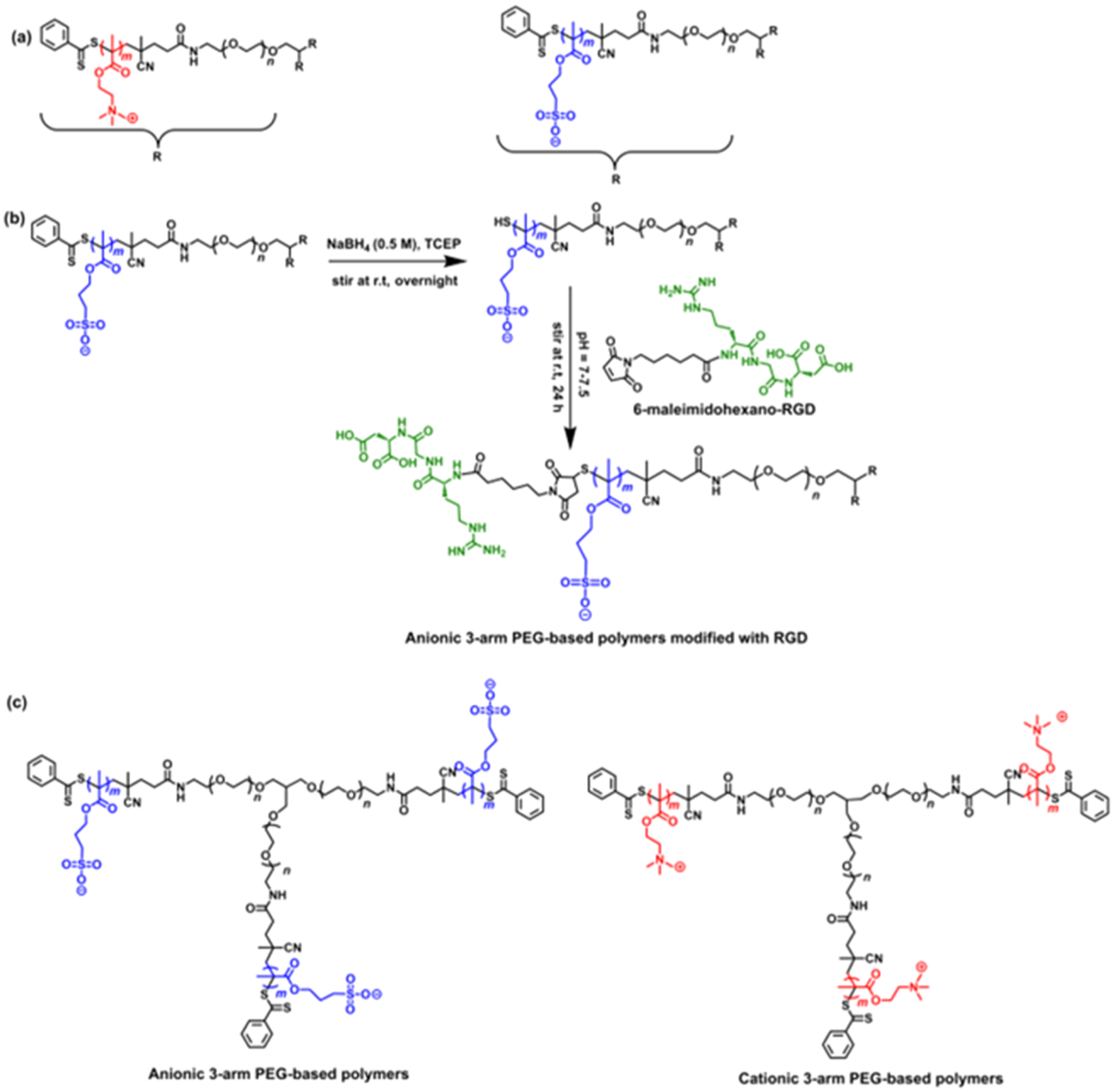

[a](a) 3-Arm PEG-based polyelectrolyte hydrogels are formed by mixing the oppositely charged polyelectrolyte polymers that are dissolved separately in a desired solution of interest at a 1:1 charge ratio. (b) The trithiocarbonate functionality of the polymer RAFT end group is reduced using $NaBH_4$ (0.5 M) and TCEP to afford polyelectrolyte 3-arm PEG-based polymers with thiol end groups. 6-Maleimidohexano-RGD was prepared via NHS coupling of RGD motifs and NHS-ester of 6-maleimidohexanoic acid in $NaHCO_3$ (50 mM, pH 8.3) at room temperature overnight. Finally, a one-pot reaction between polymer with thiol end groups and 6-maleimidohexano−RGD was carried out by stirring overnight at room temperature. The coupling reaction occurs between polyelectrolyte polymers-thiols and 6-maleimidohexano−RGD linker via the maleimide-thiol reaction to yield RGD-functionalized anionic polyelectrolytes. (c) A diagram depicting the polymer with all three arms extended.

with DPBS buffer (pre-culture staining). The stained MCF-7 cells were encapsulated in hydrogels at different polymer concentrations (10, 15, 20% w/v) containing RGD sequences or no RGD and cultured for seven days. After MCF-7 cells were encapsulated and cultured in a hydrogel for 7 days in a 5% CO_2 atmosphere at 37 °C, the medium was removed and a mixture of Apotracker and Fixable Viability Dye 620 (10 μM) was added to each well according to the procedure from the manufacturer's manual. To degrade the hydrogels, NaCl solution (2 M, 200 μL), prepared from an equal volume of 4 M NaCl and DMEM culture medium, was added to each well by gently stirring the solution by pipetting up and down for a couple of minutes. The mixture from each well was then transferred to a 96-round bottom well plate, and spheroids were spun down at 1500 rpm for 5 min. To dissociate the MCF-7 spheroids down to single cells for flow cytometry experiments, the supernatant was removed from each well and 0.25% w/v trypsin (100 μL) was added with gently breaking

https://doi.org/10.1021/acsbiomaterials.2c01252
ACS Biomater. Sci. Eng. XXXX, XXX, XXX−XXX

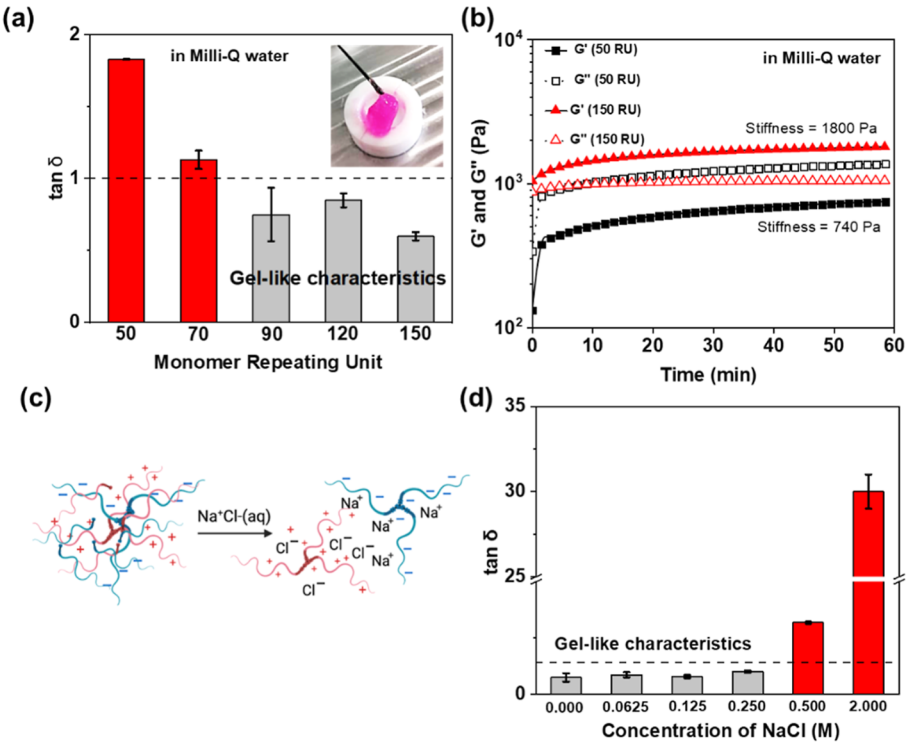

Figure 1. Effect of increasing the charged monomer RUs and ionic strength on the formation and the shear modulus of 20% w/v polyelectrolyte 3-arm PEG-based polyelectrolyte hydrogels via rheology. (a) Hydrogel-like characteristic of hydrogels made in Milli-Q water based on tan δ value < 1, where tan $\delta = G''/G'$. The polymers were prepared at a concentration of 20% (w/v) in Milli-Q water and measured at 25 and 37 °C. (b) Representative time sweeps showing hydrogel (150 RU) and non-gel-like (50 RU) characteristics. (c) Schematic representation of the dissociation of electrostatically crosslinked hydrogels in the presence of NaCl. (d) Hydrogel-like characteristics based on tan δ values when polymers with monomer RU of 90 at a polymer concentration of 20% w/v are prepared in NaCl at various concentrations (0, 0.0625, 0.125, 0.250, 0.500, and 2.000 M). n = 3 experimental replicates per group.

spheroids by pipetting up and down and incubated at 37 °C for 5−8 min until cell aggregates were not evidenced on optical microscopy. The DMEM medium (100 μL) was added to stop the trypsinization. Cells were spun down at 1500 rpm for 5 min. The supernatant was removed, and fluorescence-activated cell sorting (FACS) buffer (200 μL) was added to each well. FACS buffer (1 L) was prepared from (10× PBS buffer), Milli-Q water (900 mL), EDTA (1 mM, 292.24 mg), and FBS (2%, 20 mL). Finally, the fluorescence intensity of the stained MCF-7 cells was determined using a BD LSRFortessa flow cytometer coupled with a BD high-throughput sampler (HTS).

2.9. Statistical Analysis. The cell viability experiments were carried out in triplicates, and the data were expressed as mean ± standard deviation (SD). The results were analyzed using GraphPad Prism (version 9.3.1) and excel software to determine the statistical analysis. One-way analysis of variance technique followed by Tukey's test was applied to calculate the significance between groups. The statistical analysis was carried out at $p \leq 0.05$. At least three brightfield images were taken per hydrogel (n = 3 per condition) on a confocal microscope. The spheroid size was determined by measuring the diameter of the spheroid of the brightfield images, where at least three images were taken per hydrogel (n = 3 per condition) and a minimum of 60 spheroids were counted. All images were processed using ImageJ 1.50 (National Institutes of Health, USA). The cell viability was assessed *via* LIVE/DEAD staining. Three images were taken per hydrogel (n = 3 per condition) and processed using ImageJ 1.50 (National Institutes of Health, USA).

3. RESULTS AND DISCUSSION

3.1. Synthesis and Characterization of 3-Arm PEG-Based Hydrogels Conjugated with RGD Motifs. The synthetic polyelectrolyte 3-arm PEG-based hydrogels are prepared from two PEG-based polymers with oppositely charged end groups on each polymer chain, as depicted in Scheme 1a, such that electrostatic interaction between positively (2-(methacryloyloxy)ethyl trimethylammonium, PMAETMA) and negatively charged polymers (3-sulfopropyl methacrylate potassium salt, PSPMA) instantly forms a hydrogel. The polyelectrolyte 3-arm PEG-based polymers can be further modified with the tripeptide arginine−glycine−aspartic acid (RGD) to obtain cell-adhesive polymeric materials for cell culture applications prior to gelation. The bioconjugation of RGD was achieved in a "one-pot" reaction that comprised two steps, as shown in Scheme 1b. In the first step, the trithiocarbonate functionality of the polymer RAFT end group is reduced using 0.5 M $NaBH_4$(aq), followed by the addition of TCEP to produce 3-arm PEG-based polymeric thiols.[31] In the second step, the 6-maleimidohexano-RGD is then conjugated with the polymeric thiols to yield RGD modified 3-arm PEG-based polymers. The optimization of the reaction conditions is described in the Supporting Information. A summary of all investigated reaction parameters to obtain a 6-maleimidohexano−RGD compound is presented in Table S1. FT-IR spectroscopy was used to characterize the 6-maleimidohexano−RGD compound and RGD conjugated polymers (Figure S1). The band at 1550 cm^{-1} was attributed to the amide and N−H bending, 1660 cm^{-1} (amide, C═O stretching) and 1730 cm^{-1} (C=O stretching). These bands are the key functional groups found in NHS-ester and RGD motifs, suggesting a successful bioconjugation of RGD motif on the 3-arm PEG based-polymers.

https://doi.org/10.1021/acsbiomaterials.2c01252
ACS Biomater. Sci. Eng. XXXX, XXX, XXX−XXX

Ellman's assay was used to determine the level of free sulfhydryl moieties on the 3-arm PEG-based polymeric thiols before and after conjugation of the RGD motif by using the calibration curve of known cysteine concentration, as shown in Figure S2. The assumption is that polymers with thiol end groups react with the double bond of the maleimide on the 6-maleimidohexano−RGD compound to produce the polymers modified with RGD or referred to as "RGD-polymers". It should be noted that the Ellman's assay does not reveal any disulfide bonds that may have formed due to the free thiol ends of the polymers. However, the Ellman's assay revealed that there were adequate free thiols for conjugation to occur. The amount of thiols on the polymers that have reacted with the double bonds on maleimide corresponds directly to the polymers that are successfully modified with the RGDs. The amount of RGD conjugated to the polymers was varied by changing the number of moles of 6-maleimidohexanoic acid *N*-hydroxysuccinimide ester and RGD motifs. The results from Ellman's assay revealed that the percentage of RGD motifs on the anionic polymers could be tuned to approximately 0, 25, 75, and 98% RGD conjugation when feeding a reaction with various molar equivalent (molar equiv) of polymer/TCEP/6-maleimidohexanoic acid *N*-hydroxysuccinimide ester/RGD (Table S2). To obtain anionic polymers with 98% RGD conjugation on average, the reaction was fed with molar equiv of polymer:TCEP:ester:RGD of 1:200:6:12, respectively.

Under the same conditions that provided the anionic polymers with 98% RGD conjugation, the coupling reaction between the RGD motifs and the cationic polymers was unsuccessful, according to Ellman's assay (Table S2) and FT-IR spectrum (Figure S3). The low RGD coupling efficiency on the cationic polymers is likely to be attributed to the positively charged environment promoting hydrolysis of the succinimide ring in the linker.[32] Hence, the thiols on the polymers can no longer react to the double bond on the maleimide, making the RGD conjugation onto the cationic polymers less efficient. As an example, in one of the conditions, an extremely high amount of RGD motifs (6 times higher than a successful reaction mentioned above) was added to a reaction where molar equiv of ester and RGD were 1:200:36:72, only resulting in about (58.7 ± 3.4)% of RGD conjugation on the cationic polymers (Table S2). Since the RGD coupling reaction of cationic polymers was not shown to be as efficient as desired, henceforth, the cell adhesive RGD motif was only coupled to the anionic polymers and the cationic polymers were left unmodified.

3.2. Mechanical Properties and Degradation of 3-Arm PEG-Based Hydrogels with and without RGD Motifs. The next step was to examine the possible range of hydrogel stiffnesses with RGD and no RGD hydrogels using rheology. The effect of the lengths of the charge blocks on the formation, stability, and mechanical properties of diblock copolymeric hydrogels was first explored. The cationic and anionic polymers were synthesized with various RUs of 50, 70, 90, 120, and 150 per PEG arm. The detail of the polymerization of 3-arm PEG-based polymers with charged monomers is summarized in Table S3. The hydrogel formation of resultant polyelectrolytes made in Milli-Q water was investigated. The two polymer solutions were mixed (at a 1:1 charge ratio, a hydrogel volume of 540 μL) to form a hydrogel and the rheological properties were measured at 25 and 37 °C. A hydrogel is considered stable when its tan δ, the ratio of its liquid-like properties (loss modulus G'') and solid-like properties (storage modulus G'), is less than 1.[33] Figure 1a shows an increasing number of RU per PEG arm from 50 to 150; the electrostatically crosslinked hydrogels became stiffer with hydrogel-like characteristics observed only with polymers of at least 90 RU for hydrogels formed in Milli-Q water. Time-resolved rheology indicates how rapidly a hydrogel state is formed and the relative stiffness of the hydrogel as a function of time, shown as an example in Figure 1b. For example, the stiffnesses of a hydrogel made from polymers with 90 and 150 RU in Milli-Q water were 1529 ± 65 to 1809 ± 58 Pa, respectively (Figure 1b). Similar trends of hydrogel stiffness were obtained with forming hydrogels in DMEM and DPBS buffers (Table S4).

The stiffness of electrostatically crosslinked 3-arm PEG-based hydrogels could be tuned by varying the polymer concentration. Figure S4a,b shows that the stiffness increases as the polymer concentration increases for all three conditions, with stiffness values ranging from 280 to 1700 Pa in water and 228 to 790 Pa in the DMEM culture medium. The stiffness of these hydrogels aligns with the human endothelial, breast, and lung tissues.[34] As an example, when varying the concentrations (10, 15, and 20% w/v) of polymers with 150 RU, the stiffness values of RGD-hydrogels made in Milli-Q water changed significantly and were found to be approximately 92 ± 5 Pa (for 10% w/v polymers), 835 ± 11 Pa (15% w/v), and 1628 ± 32 Pa (20% w/v) when measured at 25 °C.

The impact of temperature on this diblock copolymeric hydrogel system was next examined. Figure S4c,d shows the hydrogel stiffness maintenance in all three conditions, with a perceptible drop in stiffness by approximately 30% when the hydrogel was heated from 25 to 37 °C for both 120 and 150 RU. Full data on hydrogel stiffness for hydrogels with and without RGD modification made in various solutions and measured at 25 and 37 °C can be found in Table S5.

To understand how salts play a role in forming the electrostatically crosslinked hydrogel system, two cell-friendly salt buffers which are DPBS without Ca^{2+} and Mg^{2+} and DMEM were used. Milli-Q water was used as salt-free control. As shown in Figure S4, the hydrogels formed from polyelectrolytes that were dissolved in Milli-Q water (no salts) exhibited the highest hydrogel stiffness, followed by the hydrogels dissolved in DPBS and DMEM. There was no statistical difference in the stiffnesses of the hydrogels among the DMEM and DPBS buffers in all three concentration groups (10, 15, and 20% w/v). These results are consistent with previous works on other polyionic-based hydrogel systems[35−37] which show that the formation of polyelectrolyte hydrogels is strongly influenced by the presence of salts in DMEM and DPBS buffers, as presented schematically in Figure 1c. The effect of the ionic strength of the salt solution on hydrogel stability was investigated. Hydrogels were formed in $CaCl_2$ and NaCl solution (0−2 M), where the ionic strength of $CaCl_2$ was three times higher than the ionic strength of NaCl. Figure 1d represents hydrogel and non-hydrogel-like characteristics based on the tan δ values when 3-arm PEG-based polymers were dissolved in NaCl solutions. In a control group, polyelectrolyte polymers with 90 RU, prepared in Milli-Q water [0 M (Figure S5a)], show hydrogel-like characteristics over 60 min. In contrast, when dissolving polyelectrolyte polymers in 0.500 M NaCl as an example (Figure S5b), a change in mechanical behavior from solid-like to liquid-like was observed, where the G'' value is higher than the G' value.

https://doi.org/10.1021/acsbiomaterials.2c01252
ACS Biomater. Sci. Eng. XXXX, XXX, XXX−XXX

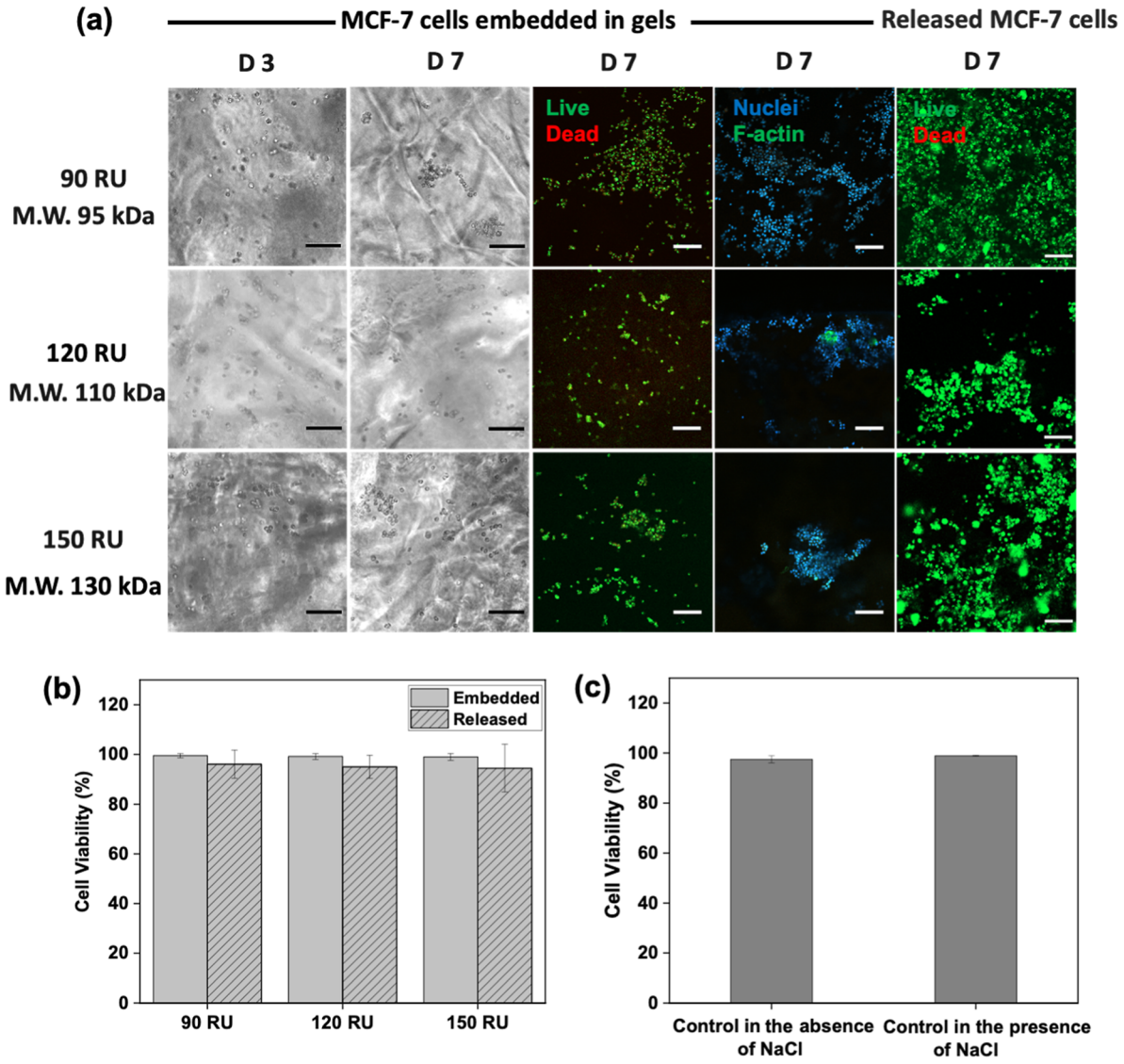

Figure 2. Cell viability of MCF-7 embedded within a hydrogel at 20% w/v and after released from a hydrogel using 2 M NaCl solution. (a) Representative brightfield and fluorescence images of MCF-7 breast cancer cells cultured in unmodified 3-arm PEG-based polyelectrolyte hydrogel with different polymer molecular weights (95, 110, and 130 kDa at 20% w/v polymer concentration). Cells were stained with calcein-AM (LIVE, green) and ethidium homodimer (DEAD, red), phalloidin (cell F-actin microfilament, green), and Hoechst 33342 (cell nucleus, blue) on day 7. Initial seeding density of 5.0×10^6 cells/mL. All scale bars 100 μm. $n = 3$ experimental replicates per group. (b,c) Cell viability (in percentage, %) of MCF-7 assessed by LIVE/DEAD assay. The columns represent the mean ± SD ($n = 3$). There were no significant differences in viability when MCF-7 cells were embedded in a hydrogel, released from a hydrogel, cultured on 2D for 48 h (a control group in the absence of NaCl), or treated directly with 2 M NaCl on 2D for 5 min (a control group in the presence of NaCl).

To explore whether the dicationic species have a more pronounced effect on the formation of the hydrogels, due to the ionic strength, polymers were prepared in $CaCl_2$ solution. The results showed that when changing the solution from NaCl to $CaCl_2$ (Figure S6), hydrogels made in $CaCl_2$ at the same concentration of 0.0625 M produce a hydrogel with lower stiffness (800 Pa) compared to when making a hydrogel in NaCl (1331 Pa). In fact, at a concentration of 0.0625 M, rheology shows non-hydrogel-like characteristics for hydrogels that were made in $CaCl_2$ while the one in NaCl still showed hydrogel-like behavior. Swelling behavior (Figure S4) and mesh size (Table S3) were also calculated, and no significant difference was observed for either parameters when changing concentration or RU length.

3.3. Cytocompatibility of Hydrogel and the Release of Embedded Cells from Hydrogels. The next step was to investigate the capability of using this hydrogel system as an ECM mimic for 3D cell culture applications. The cytocompatibility of the hydrogel was first determined by encapsulating MCF-7 cells within a 3-arm PEG-based hydrogel made from different molecular weights (by changing monomer charge block lengths) and cultured for 7 days with an initial cell seeding density of 2.4×10^6 cells/mL. Representative brightfield images of MCF-7 cells grown in hydrogels showed small clusters of MCF-7 cells on day 3 and day 7 (Figure 2a). All three PEG hydrogels showed high cytocompatibility using LIVE/DEAD assay to evaluate cell viability in each hydrogel condition. LIVE/DEAD images (Figure 2a) reveal that MCF-7 cells remained viable after 7 days of culture with cell viability of 99.5 ± 0.8, 99.1 ± 1.2 and 99.0 ± 1.4% in hydrogels with molecular weight of 95, 110, and 130 kPa, respectively (Figure 2b). This indicates that this hydrogel system is highly

https://doi.org/10.1021/acsbiomaterials.2c01252
ACS Biomater. Sci. Eng. XXXX, XXX, XXX−XXX

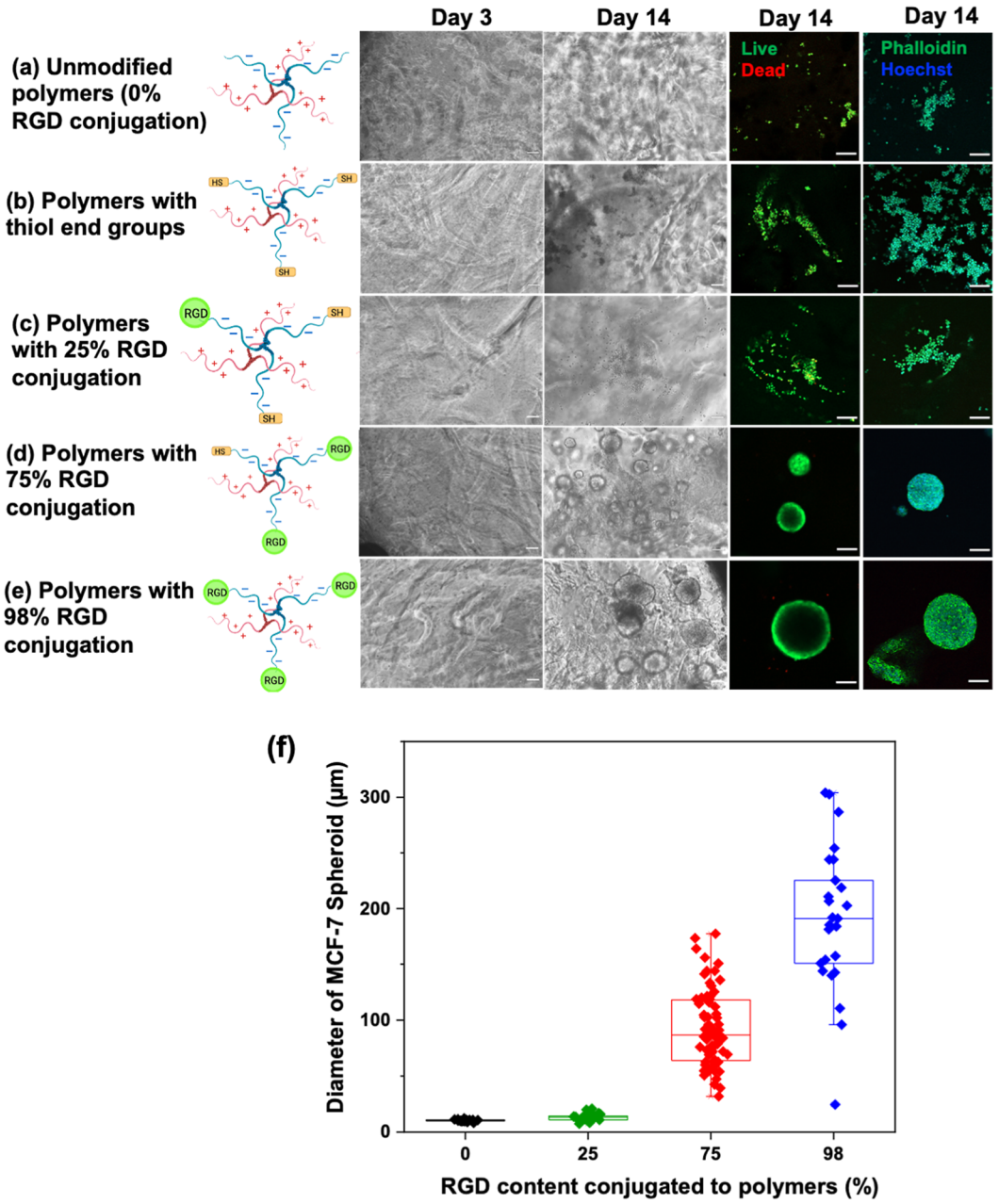

Figure 3. Brightfield and fluorescence images showing the growth and morphology of MCF-7 cells embedded within 90 RU polyelectrolyte 3-arm PEG-based hydrogel in various RGD peptide content over 14 days. (a) 0% (unmodified gel), (b) 0% [polymers with thiol (−SH) end group], (c) 25% RGD, (d) 75% RGD, and (e) 98% RGD. An initial seeding density of MCF-7 cells was 2.5×10^6 cells/mL. Hydrogels were prepared from polymers with 90 RU (M.W. = 95 kDa) at a polymer concentration of 20% w/v which were then dissolved in a DMEM culture medium prior to making a hydrogel. Cell F-actin microfilament was stained with phalloidin (green); cell nucleus was counterstained with Hoechst 33342 (blue). Scale bars: 100 μm. (f) Diameter of MCF-7 spheroids at day 14 was measured from brightfield images using ImageJ software. n = 3 experimental replicates per group.

cytocompatible with the potential to serve as an ECM scaffolding material.

As presented above, the electrostatically crosslinked hydrogels can be dissociated by exposing the hydrogels to electrolytes with a sufficiently high concentration that can shield the electrostatic interaction of the charges on the polymer chains. We, therefore, sought to ask the question, can high electrolyte concentrations be used to dissociate the hydrogels to release cells for the ECM mimic without compromising their viability. Table S6 shows that the minimal volume of 200 μL of 2 M NaCl solution was enough to fully disintegrate a 50 μL hydrogel within 30 s by gently breaking it apart with a pipette tip which is consistent with rheology data, as shown previously in Figure 1d. As such, the MCF-7 cells were released from the polyelectrolyte hydrogel with a 2 M NaCl solution. LIVE/DEAD staining was then used to evaluate MCF-7 cell viability after being released from a hydrogel. LIVE/DEAD images in Figure 2a reveals that MCF-7 cells remained viable after being released from a hydrogel with cell viabilities of 96.1 ± 5.7, 95.0 ± 4.7, and 94.4 ± 9.6% in hydrogels with molecular weights of 95, 110, and 130 kPa, respectively (Figure 2b). The viability of released MCF-7 cells

https://doi.org/10.1021/acsbiomaterials.2c01252
ACS Biomater. Sci. Eng. XXXX, XXX, XXX−XXX

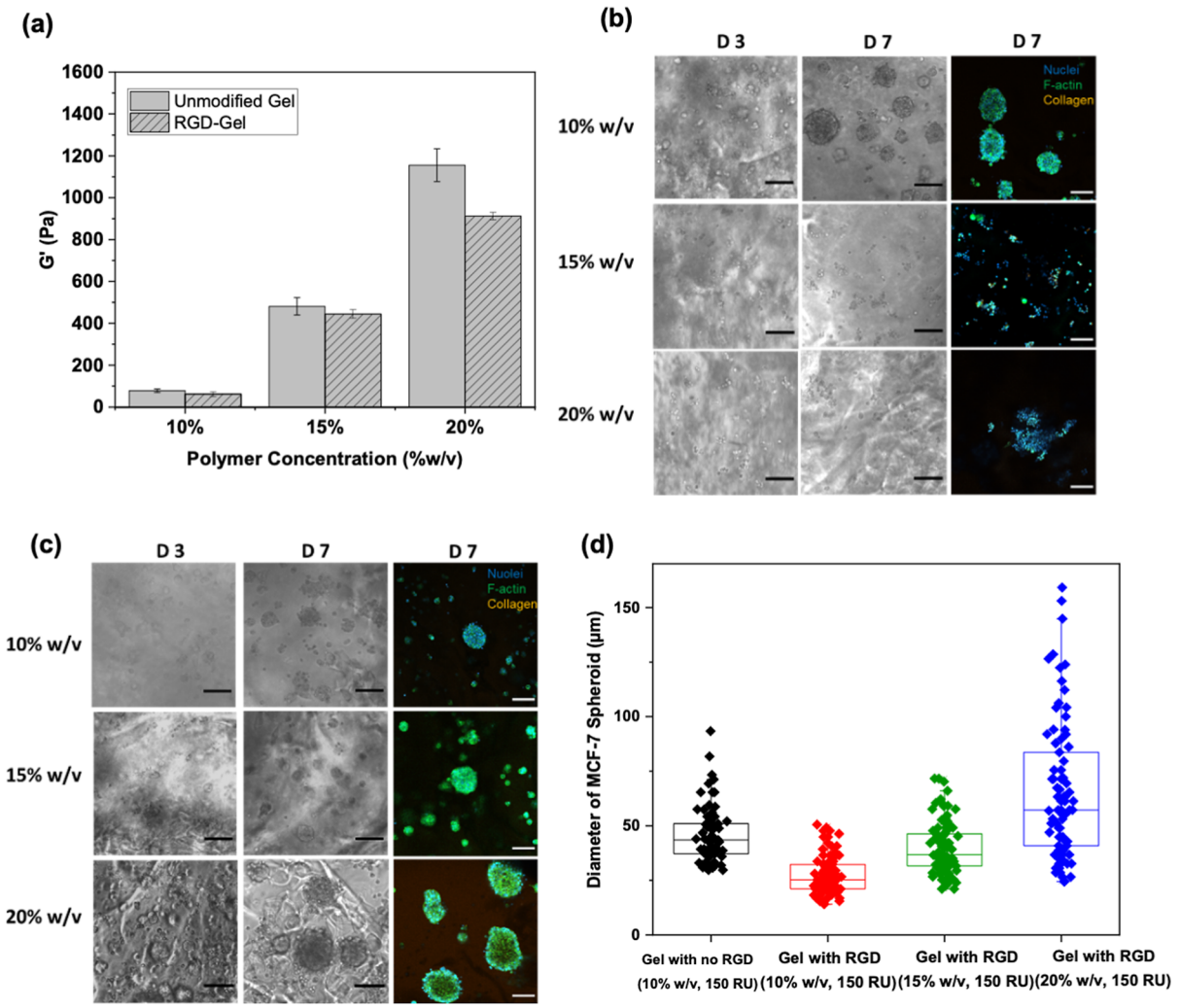

Figure 4. Formation of MCF-7 breast cancer spheroids in electrostatically crosslinked 150 RU 3-arm PEG-based hydrogel with various hydrogel stiffness by changing polymer concentrations with a fixed polymer molecular weight of 130 kDa. (a) Storage moduli (hydrogel stiffness) were characterized using bulk oscillatory rheology at 37 °C. MCF-7 cells were embedded in hydrogels with (b) no RGD and (c) RGD motifs (98%), where hydrogels were made from polymers with 130 kDa at a concentration of 10, 15, and 20% w/v. (d) Diameter of formed MCF-7 spheroids at day 7 in each condition, with a minimum of 60 spheroids, were counted using ImageJ software. Initial cell seeding density of 5.0×10^6 cells/mL. All scale bars, 100 μm. $n = 3$ experimental replicates per group.

was compared with respect to the controls. Figure 2c shows the viability of MCF-7 cells in the absence and presence of 2 M NaCl solution, where cell viability was maintained: 98.9 ± 0.2 and 97.5 ± 1.4%, respectively. LIVE/DEAD images of the control groups can be seen in Figure S7. In brief, there were no significant differences in cell viability when MCF-7 cells were embedded in a hydrogel, released from a hydrogel, cultured on 2D, or treated directly with 2 M NaCl on 2D. Therefore, the results confirmed that 2 M NaCl could safely and effectively release cells from a polyelectrolyte 3-arm PEG-based ECM scaffolding hydrogel.

3.4. Influence of RGD Content on Spheroid Formation of MCF-7 Cells. Next, polymers with a varied amount of RGD content characterized earlier were used to form hydrogels to study the influences of increasing amounts of RGD on cell adhesion and MCF-7 breast cancer spheroid formation. This was performed by using gels with 90 RU and 20% w/v with 0, 25, 75, and 98% of the thiol handles functionalized with RGD. To explore how the RGD content affects the organization of MCF-7 cells into spheroids, MCF-7 breast cancer cells were embedded and incubated within a hydrogel containing various RGD content for 14 days (Figure 3a–e), with an initial cell seeding density of 2.5×10^6 cells/mL. Figure 3f presents the diameter of cell aggregates of MCF-7 cells where spheroids were observed on day 14 for 75% RGD-hydrogels ($n = 75$) and 98% RGD-hydrogels ($n = 30$) with an average diameter of 92.2 ± 33.1 and 190.2 ± 65.0 μm, respectively. This observation is consistent with other embedded MCF-7 studies where cells fused to form spheroids.[38−40] The process of spheroid formation involves three stages: (1) formation of loose cell aggregates *via* integrin-ECM binding. RGD-containing binding sites for cell−surface integrins can promote this step to achieve rapid cell aggregation;[41,42] (2) after the early aggregation stage, E-cadherin, which is a cell−cell adhesion protein fulfilling a prominent role in epithelial differentiation,[43] plays a major role in cell cohesion and adhesion through homophilic cadherin−cadherin binding between two adjacent cells;[42,44] (3) an accumulation of E-cadherin induces cell compactness which eventually leads to spheroid formation.[42,45] Note only small

https://doi.org/10.1021/acsbiomaterials.2c01252
ACS Biomater. Sci. Eng. XXXX, XXX, XXX−XXX

clusters of MCF-7 cells, rather than spheroids, were observed with the 0 and 25% conjugated RGD groups, even after 14 days, while with 75 and 98% RGD, well-defined spheroids are formed (Figure 3a–e). These observations confirmed that RGD can facilitate spheroid formation through cell aggregation *via* RGD-containing binding sites for cell–surface integrins.

With the 98% RGD polymer, spheroids of size 200 μm or more exhibited in vivo-like necrotic cores;[46,47] therefore, the rest of studies we focused on using the unmodified polymers and polymers with 98% RGD conjugation will henceforth be now referred to as RGD-hydrogel.

To enhance and quicken biological screening, the culture time was reduced from 14 days to 7 days and cell density was increased from 2.5×10^6 and 5.0×10^6 cells/mL for the rest of the studies. It was found that the size of MCF-7 spheroids on day 7 in the hydrogel with RGD was approximately 2.5 times bigger (116.0 ± 38.2 μm) with a higher cell density (5.0×10^6 cells/mL) compared to a lower cell density group (2.5×10^6 cells/mL) where the average spheroid size was 46.0 ± 11.3 μm (Figure S8). Polymers conjugated with RDG were also explored (Figure S9), and spheroids were observed in 10 and 15% w/v gels but not in the 20% w/v which is the stiffest condition. As seen in Table S7, spheroids also formed in the softest of the unmodified gels at a concentration of 10% w/v. This suggests that in the absence of RGD, the MCF-7 cells more readily form spheroids in the softer gels but not in stiffer conditions.

3.5. Influence of Hydrogel Stiffness on Spheroid Formation of MCF-7 Cells. Next, the influence of stiffness on spheroid formation was investigated. The stiffness was adjusted by changing the 150 RU polymer concentrations which have a fixed polymer molecular weight of 130 kDa. MCF-7 cells were encapsulated within the polyelectrolyte 3-arm PEG-based hydrogels from polyelectrolyte concentrations of 10, 15, and 20% w/v and cultured for 7 days. Rheology of PEG-hydrogels containing RGD measured stiffnesses of approximately 62.3 ± 10.8, 444.5 ± 20.7, and 912.1 ± 17.3 Pa for 10, 15, and 20% w/v, respectively, at 37 °C (Figure 4a and Table S7) which align with the stiffness of human breasts and lungs and tissues.[34] There was no significant difference in stiffness between unmodified hydrogels and those modified with RGD.

Immunostaining images in Figure 4b reveal that spheroids of MCF-7 cells only formed in softer (10% w/v) but not the stiffer hydrogels (15 and 20% w/v) when embedding in hydrogels with no RGD. This is consistent with previous studies which reported that spheroids of MCF-7 cells had formed without additional stimuli such as any binding motif[42,48–50] in soft hydrogels (600 Pa).[51] In contrast, Figure 4c reveals that MCF-7 cell spheroids had formed in hydrogels with RGD modification for all three polymer concentrations. Spheroid formation of encapsulated MCF-7 cells in RGD-hydrogels. It was previously reported that cell migration is inhibited in stiffer 3D hydrogels.[52] However, the adhesive peptides such as RGD can promote cell aggregation through cell–surface integrins and facilitate cell adhesion and migration[53,54] Through the early aggregation stage and E-cadherin accumulation, spheroid formation occurs as discussed previously.[41,42,44,45] For the groups where spheroids had formed, the MCF-7 growth was then quantified by measuring the diameter of spheroids (brightfield images) on day 7. Figure 4d shows that at day 7, MCF-7 spheroids were larger with an average size of 42.1 ± 12.4 μm ($n = 63$) when cultured in softer RGD-hydrogels (84.3 Pa, 10% w/v polymer concentration) compared to the stiffer RGD-hydrogels (386 Pa, 15% w/v polymer concentration) which produced most spheroid populations with a diameter of 37.8 ± 8.7 μm ($n = 67$). The size of the spheroid here is comparable to previous work, where MCF-7 cells were cultured for 7 days in other soft hydrogels.[55] The noticeable difference in size compared to those observed in Figure 3 is due to the length of culture time. While we have indirect evidence that the cells can freely migrate in the hydrogel, particularly when presented with cell adhesion peptides, more work is necessary to understand the modes of cancer cell migration in this new class of soft material.

3.6. Release of Embedded Spheroids of MCF-7 Cells from Hydrogels for Flow Cytometry. Next, spheroids of MCF-7 embedded for 7 days were released from the 3-arm PEG hydrogel using a 2 M NaCl solution. LIVE/DEAD images (Figure 5a) confirm that the released spheroids

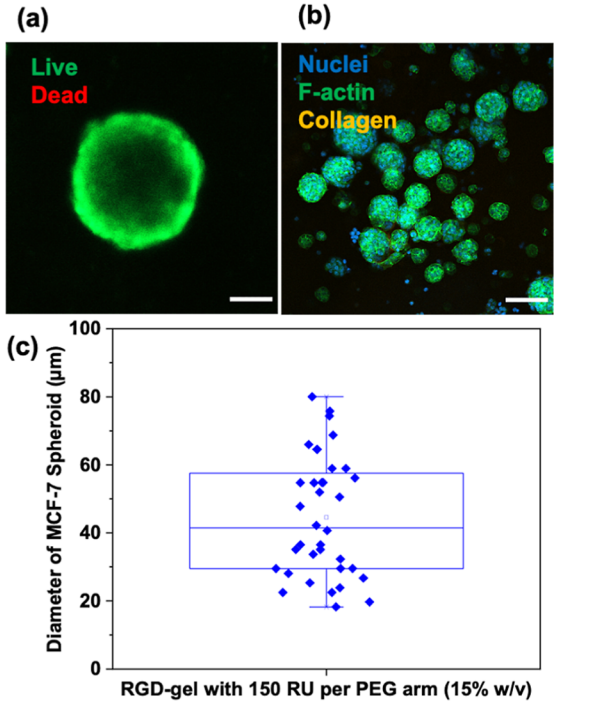

Figure 5. Release of MCF-7 breast cancer spheroids from 3-arm PEG-based polyelectrolyte hydrogels using 2 M NaCl (aq). Cell viability of MCF-7 cells after being released from a hydrogel was tested at day 7. (a) LIVE/DEAD fluorescence images of the released spheroids. Spheroids were stained with calcein-AM (Live, green) and ethidium homodimer (Dead, red); (b) Immunostaining fluorescence images of the released spheroids. Cell F-actin microfilament was stained with phalloidin (green); cell nucleus was counterstained with Hoechst 33342 (blue); (c) Diameter of the released MCF-7 spheroids was measured from brightfield images at day 7 using ImageJ. All scale bars 100 μm. $n = 3$ experimental replicates per group.

remained viable after being treated with a 2 M NaCl solution for 5 min to release them from the hydrogel. The diameter of released spheroids was measured from brightfield images and was found to be approximately 50.5 ± 16.0 μm ($n = 84$). Immunostaining images (Figure 5b) show that a single spheroid remained intact throughout the electrolyte treatment. Spheroids were still densely packed with compact nuclei clusters, and the edge of the MCF-7 cell aggregates retained

https://doi.org/10.1021/acsbiomaterials.2c01252
ACS Biomater. Sci. Eng. XXXX, XXX, XXX–XXX

their shape. F-actin networks formed within spheroids during spheroid formation were still present even after being treated with a 2 M NaCl solution. The ability to release the spheroid is very encouraging to explore its potential for downstream analysis which is discussed in the next section.

The facile release of cells and spheroids from the ECM mimic 3-arm hydrogel provides an opportunity to recover cells for downstream assays such as characterization *via* flow cytometry. To evaluate this potential, MCF-7 cells were stained with 10 μM CellTrace Violet before cell culture in hydrogels with different stiffness through changing polymer concentrations (10, 15, and 20% w/v), resulting in hydrogels with stiffnesses of 80, 480, and 1160 Pa, respectively. As discussed above, seven-day culture spheroids were retrieved from 3D hydrogels using a 2 M NaCl solution. Spheroids were then dissociated into single-cell suspensions using a 0.25% w/v trypsin−EDTA solution. Cells were also stained with cell-impermeant DNA dye (Fixable Viability Dye 620) before being released from hydrogel to estimate MCF-7 cell viability at day 7. Figure S10a shows a representative graph of cell viability and proliferation of MCF-7 cells at day 7. A CellTrace Violet signal measured a decrease in the geometric median of fluorescence intensity of cells as it proliferates over 7 days of culture. The lower the intensity in the signal from the CellTrace violet assay indicates, the higher the proliferation of cells as the fluorescent dye contained in MCF-7 cells is split into the next generations when cells divide.[56] The proliferation of MCF-7 cells was found to be lower, as the intensity of the CellTrace Violet signal remained relatively higher, with an increase in hydrogel stiffness for hydrogels with no RGD (Figure S10b). This aligns with the previous report, indicating that cancer cells prefer and proliferate better in softer hydrogel scaffolds when embedded and grown in a 3D environment.[57] In contrast, Figure S10c shows that MCF-7 cells tend to proliferate more in stiffer hydrogels (445 and 910 Pa) compared to softer hydrogels (60 Pa) when embedding cells in RGD conjugated hydrogels. It was also observed that with similar hydrogel stiffness, cells embedded in hydrogels containing RGD proliferated more, according to the lower fluorescence intensity, than no RGD hydrogels made from the same polymer concentration (Figure S10b,c). These results point to the role of RGD in promoting the proliferation of MCF-7 cells in a 3D hydrogel environment, consistent with previous studies,[8] that show hydrogel with RGD adhesive peptide effectively promotes the proliferation of endothelial cells.[58−60]

A detailed estimation of cell viability was then performed by measuring apoptotic/necrosis (annexin V) and plasma membrane integrity (cell-impermeable DNA dye) (Figure S11). Red arrows in each quadrant represent the cell population exhibiting different stages of apoptosis: viable cells in Q4, apoptosis and necrotic (Q3) and dead (Q2) cells which are characterized by the exposure of Annexin V and DNA to cell-impermeant staining reagents. After a prolonged injury, the integrity of the plasma membrane is disrupted, allowing DNA staining by viable dye as well as intra- and extracellular Annexin V staining, resulting in a double-positive cell population. Cell viability of the 2D cell culture control group with no dye is shown in Figure S11a. Figure S11b is a representative graph of MCF-7 cell viability at day 7 after being released from hydrogels with or without the RGD motif. Figure S11c,d reveals that there were no significant differences in the percentage of live cells (Q4), apoptotic/necrotic cells (Q3), early death cells (Q2), and dead cells (Q1) for both hydrogel groups containing RGD or no RGD motif across 3 hydrogel stiffness made from polymer concentrations of 10, 15, and 20%. The percentages of the cell population for each group were approximately 85.3 ± 6.2% (Q4, live cells), 3.8 ± 1.4% (Q3, apoptotic cells), and 10.7 ± 5.1% (Q2, early death/dead cells). These results suggest that the stiffness of hydrogel in a range between 60 to 1160 Pa does not influence the viability of MCF-7 cells. This aligns with prior reports, which found that the cellular viability of MCF-7 cells is not due to the stiffness of hydrogel, especially when the stiffness is under 1000 Pa.[61,62] In addition, there is no statistically significant difference in cell viability cultured in hydrogels either with or without the RGD motif. This is consistent with a previous work by Burdick and Anseth, which showed that the cell viability of encapsulated rat calvarial osteoblasts did not significantly improve by modifying the hydrogel network with RGD.[63] Huang et al. also reported that MCF-7 cells remained highly viable cultured, and the 3D culture conditions induced no significant apoptosis over 7 days.[55]

4. CONCLUSIONS

This work provides knowledge toward understanding the formation, stability, and mechanical properties of electrostatically crosslinked 3-arm PEG-based hydrogels to embed and release breast cancer spheroids. The ability to tune the degree of RGD content (0, 25, 75, and 98%) on the polyelectrolyte 3-arm PEG-based polymer chains was shown. In addition, the results revealed that this hydrogel system is cytocompatible and suitable to be used as an ECM mimic when tested against MCF-7 breast cancer cells that maintain high cell viability (99.0 ± 1.4)%. Furthermore, the capability of using the electrostatically crosslinked 3-arm PEG-based hydrogels to release MCF-7 cells and spheroids at any desired time points by simply exposing the hydrogels to 2 M NaCl solution for potential further downstream analysis without compromising cell viability was demonstrated. The results showed that the released MCF-7 cells remained highly viable. Flow cytometric experiments revealed that MCF-7 cells prefer and proliferate more in softer hydrogel scaffolds than stiffer ones when embedded and grown in a 3D environment. The RGD motif plays a role in promoting the proliferation of MCF-7 cells as hydrogels get stiffer. Moreover, the viability of MCF-7 was not shown to be influenced by the stiffness of hydrogel in a range between 60 and 1160 Pa. Taken together, this hydrogel system can be used as an ECM mimic in 3D cell culture applications for downstream analysis of biological events, such as the cell−cell and cell−matrix interactions, at bulk- and single-cell levels, a feature that can be difficult to achieve with other synthetic hydrogel systems. Additionally, this polymer system should be compatible with a drop-on-demand 3D bioprinter, where cationic and anionic polymers can be used as bioinks and printed alternatingly, to produce 3D cell cultures in a high-throughput manner where statistically relevant data can be obtained.

■ ASSOCIATED CONTENT

Supporting Information

The Supporting Information is available free of charge at https://pubs.acs.org/doi/10.1021/acsbiomaterials.2c01252.

Details of polymer synthesis and characterization, additional cell data, and flow cytometry data (PDF)

https://doi.org/10.1021/acsbiomaterials.2c01252
ACS Biomater. Sci. Eng. XXXX, XXX, XXX−XXX

AUTHOR INFORMATION

Corresponding Author

J. Justin Gooding − *School of Chemistry, UNSW, Sydney, New South Wales 2052, Australia; Australian Centre for NanoMedicine, UNSW, Sydney, New South Wales 2052, Australia;* orcid.org/0000-0002-5398-0597; Phone: +61 (2) 9385 5384; Email: justin.gooding@unsw.edu.au

Authors

Panthipa Suwannakot − *School of Chemistry, UNSW, Sydney, New South Wales 2052, Australia; Australian Centre for NanoMedicine, UNSW, Sydney, New South Wales 2052, Australia*

Stephanie Nemec − *School of Materials Science and Engineering, UNSW, Sydney, New South Wales 2052, Australia*

Newton Gil Peres − *School of Medical Sciences, EMBL Australia Node in Single Molecule Science, UNSW, Sydney, New South Wales 2052, Australia*

Eric Y. Du − *School of Chemistry, UNSW, Sydney, New South Wales 2052, Australia; Australian Centre for NanoMedicine, UNSW, Sydney, New South Wales 2052, Australia*

Kristopher A. Kilian − *School of Chemistry, UNSW, Sydney, New South Wales 2052, Australia; School of Materials Science and Engineering and Australian Centre for NanoMedicine, UNSW, Sydney, New South Wales 2052, Australia;* orcid.org/0000-0002-8963-9796

[#]Katharina Gaus − *School of Medical Sciences, EMBL Australia Node in Single Molecule Science, UNSW, Sydney, New South Wales 2052, Australia*

Maria Kavallaris − *Children's Cancer Institute, Lowy Cancer Research Centre and Australian Centre for NanoMedicine, UNSW, Sydney, New South Wales 2052, Australia*

Complete contact information is available at: https://pubs.acs.org/10.1021/acsbiomaterials.2c01252

Author Contributions

P.S., S.N., J.J.G. designed the experiments. P.S. synthesized and characterized the mechanical properties of materials. P.S. and S.N. designed, performed, and analyzed cellular experiments. N.G.P. and P.S. performed and analyzed flow cytometry experiments. J.J.G., M.K., K.G., and K.K. interpreted the data and provided feedback. All authors contributed to writing the manuscript and have approved the final version of the manuscript.

Notes

The authors declare no competing financial interest.

[#]Deceased.

ACKNOWLEDGMENTS

We acknowledge the Australian Research Council (ARC) Linkage Grant (LP170100623 J.J.G., M.K.) and the National Health and Medical Research Council (NHMRC) for a Project Grant (GNT11662385 to J.J.G., K.G.) and an NHMRC Investigator (GNT1196648). We acknowledge the facilities and the scientific and technical support of staff at the Katharina Gaus Light Microscopy Facility at UNSW Sydney. Some figures were created using BioRender.

REFERENCES

(1) Abbott, A. *Biology's New Dimension*; Nature Publishing Group, 2003.

(2) Debnath, J.; Brugge, J. S. Modelling glandular epithelial cancers in three-dimensional cultures. *Nat. Rev. Cancer* **2005**, *5*, 675.

(3) Weigelt, B.; Bissell, M. J. Unraveling the microenvironmental influences on the normal mammary gland and breast cancer. *Semin. Cancer Biol.* **2008**, *18*, 311−321.

(4) Liu, S. Q.; Tay, R.; Khan, M.; Rachel Ee, P. L. R.; Hedrick, J. L.; Yang, Y. Y. Synthetic hydrogels for controlled stem cell differentiation. *Soft Matter* **2010**, *6*, 67−81.

(5) Cushing, M. C.; Anseth, K. S. Hydrogel cell cultures. *Science* **2007**, *316*, 1133−1134.

(6) Aisenbrey, E. A.; Murphy, W. L. Synthetic alternatives to Matrigel. *Nat. Rev. Mater.* **2020**, *5*, 539−551.

(7) Kloxin, A. M.; Kloxin, C. J.; Bowman, C. N.; Anseth, K. S. Mechanical properties of cellularly responsive hydrogels and their experimental determination. *Adv. Mater.* **2010**, *22*, 3484−3494.

(8) Ruoslahti, E.; Pierschbacher, M. D. New perspectives in cell adhesion: RGD and integrins. *Science* **1987**, *238*, 491−497.

(9) Junutula, J. R.; Raab, H.; Clark, S.; Bhakta, S.; Leipold, D. D.; Weir, S.; Chen, Y.; Simpson, M.; Tsai, S. P.; Dennis, M. S.; Lu, Y.; Meng, Y. G.; Ng, C.; Yang, J.; Lee, C. C.; Duenas, E.; Gorrell, J.; Katta, V.; Kim, A.; McDorman, K.; Flagella, K.; Venook, R.; Ross, S.; Spencer, S. D.; Lee Wong, W.; Lowman, H. B.; Vandlen, R.; Sliwkowski, M. X.; Scheller, R. H.; Polakis, P.; Mallet, W. Site-specific conjugation of a cytotoxic drug to an antibody improves the therapeutic index. *Nat. Biotechnol.* **2008**, *26*, 925.

(10) Bryant, S. J.; Anseth, K. S.; Lee, D. A.; Bader, D. L. Crosslinking density influences the morphology of chondrocytes photoencapsulated in PEG hydrogels during the application of compressive strain. *J. Orthop. Res.* **2004**, *22*, 1143−1149.

(11) Soman, P.; Kelber, J. A.; Lee, J. W.; Wright, T. N.; Vecchio, K. S.; Klemke, R. L.; Chen, S. Cancer cell migration within 3D layer-by-layer microfabricated photocrosslinked PEG scaffolds with tunable stiffness. *Biomaterials* **2012**, *33*, 7064−7070.

(12) Miyata, T.; Uragami, T.; Nakamae, K. Biomolecule-sensitive hydrogels. *Adv. Drug Delivery Rev.* **2002**, *54*, 79−98.

(13) Lee, J.; Cuddihy, M. J.; Kotov, N. A. Three-dimensional cell culture matrices: state of the art. *Tissue Eng., Part B* **2008**, *14*, 61−86.

(14) Maitra, J.; Shukla, V. K. Cross-linking in hydrogels-a review. *Am. J. Polym. Sci.* **2014**, *4*, 25−31.

(15) Garavand, F.; Rouhi, M.; Razavi, S. H.; Cacciotti, I.; Mohammadi, R. Improving the integrity of natural biopolymer films used in food packaging by crosslinking approach: A review. *Int. J. Biol. Macromol.* **2017**, *104*, 687−707.

(16) Huang, Q.; Zou, Y.; Arno, M. C.; Chen, S.; Wang, T.; Gao, J.; Dove, A. P.; Du, J. Hydrogel scaffolds for differentiation of adipose-derived stem cells. *Chem. Soc. Rev.* **2017**, *46*, 6255−6275.

(17) Hospodiuk, M.; Dey, M.; Sosnoski, D.; Ozbolat, I. T. The bioink: A comprehensive review on bioprintable materials. *Biotechnol. Adv.* **2017**, *35*, 217−239.

(18) Utama, R. H.; Tan, V. T.; Tjandra, K. C.; Sexton, A.; Nguyen, D. H.; O'Mahony, A. P.; Du, E. Y.; Tian, P.; Ribeiro, J. C.; Kavallaris, M.; Gooding, J. J. A Covalently Crosslinked Ink for Multimaterials Drop-on-Demand 3D Bioprinting of 3D Cell Cultures. *Macromol. Biosci.* **2021**, *21*, 2100125.

(19) Utama, R. H.; Atapattu, L.; O'Mahony, A. P.; Fife, C. M.; Baek, J.; Allard, T.; O'Mahony, K. J.; Ribeiro, J. C.; Gaus, K.; Kavallaris, M.; Gooding, J. J. A 3D bioprinter specifically designed for the high-throughput production of matrix-embedded multicellular spheroids. *iScience* **2020**, *23*, 101621.

(20) Li, Y.; Chen, X.; Jin, R.; Chen, L.; Dang, M.; Cao, H.; Dong, Y.; Cai, B.; Bai, G.; Gooding, J. J.; Liu, S.; Zou, D.; Zhang, Z.; Yang, C. Injectable hydrogel with MSNs/microRNA-21-5p delivery enables both immunomodification and enhanced angiogenesis for myocardial infarction therapy in pigs. *Sci. Adv.* **2021**, *7*, No. eabd6740.

(21) Nguyen, D. H. T.; Utama, R. H.; Tjandra, K. C.; Suwannakot, P.; Du, E. Y.; Kavallaris, M.; Tilley, R. D.; Gooding, J. J. Tuning the mechanical properties of multi-arm RAFT-based block co-polyelectrolyte hydrogels via ionic crosslinking for 3D cell cultures. *Biomacromolecules* **2023**, *24*, 57−68.

(22) He, X.; Jabbari, E. Material Properties and Cytocompatibility of Injectable MMP Degradable Poly(lactide ethylene oxide fumarate) Hydrogel as a Carrier for Marrow Stromal Cells. *Biomacromolecules* **2007**, *8*, 780−792.
(23) Zhang, J.; Skardal, A.; Prestwich, G. D. Engineered extracellular matrices with cleavable crosslinkers for cell expansion and easy cell recovery. *Biomaterials* **2008**, *29*, 4521−4531.
(24) Peng, K.; Tomatsu, I.; van den Broek, B.; Cui, C.; Korobko, A. V.; van Noort, J.; Meijer, A. H.; Spaink, H. P.; Kros, A. Dextran based photodegradable hydrogels formed via a Michael addition. *Soft Matter* **2011**, *7*, 4881−4887.
(25) Tibbitt, M. W.; Han, B. W.; Kloxin, A. M.; Anseth, K. S. Synthesis and application of photodegradable microspheres for spatiotemporal control of protein delivery. *J. Biomed. Mater. Res., Part A* **2012**, *100*, 1647.
(26) Kaihara, S.; Matsumura, S.; Fisher, J. P. Synthesis and properties of poly [poly (ethylene glycol)-co-cyclic acetal] based hydrogels. *Macromolecules* **2007**, *40*, 7625−7632.
(27) Falco, E. E.; Patel, M.; Fisher, J. P. Recent developments in cyclic acetal biomaterials for tissue engineering applications. *Pharm. Res.* **2008**, *25*, 2348−2356.
(28) Mahoney, M. J.; Anseth, K. S. Three-dimensional growth and function of neural tissue in degradable polyethylene glycol hydrogels. *Biomaterials* **2006**, *27*, 2265−2274.
(29) Rice, M. A.; Anseth, K. S. Controlling cartilaginous matrix evolution in hydrogels with degradation triggered by exogenous addition of an enzyme. *Tissue Eng.* **2007**, *13*, 683−691.
(30) Bryant, S. J.; Anseth, K. S. Hydrogel properties influence ECM production by chondrocytes photoencapsulated in poly(ethylene glycol) hydrogels. *J. Biomed. Mater. Res.* **2002**, *59*, 63−72.
(31) Scales, C. W.; Convertine, A. J.; McCormick, C. L. Fluorescent labeling of RAFT-generated poly (N-isopropylacrylamide) via a facile maleimide− thiol coupling reaction. *Biomacromolecules* **2006**, *7*, 1389−1392.
(32) Shen, B.-Q.; Xu, K.; Liu, L.; Raab, H.; Bhakta, S.; Kenrick, M.; Parsons-Reponte, K. L.; Tien, J.; Yu, S.-F.; Mai, E.; Li, D.; Tibbitts, J.; Baudys, J.; Saad, O. M.; Scales, S. J.; McDonald, P. J.; Hass, P. E.; Eigenbrot, C.; Nguyen, T.; Solis, W. A.; Fuji, R. N.; Flagella, K. M.; Patel, D.; Spencer, S. D.; Khawli, L. A.; Ebens, A.; Wong, W. L.; Vandlen, R.; Kaur, S.; Sliwkowski, M. X.; Scheller, R. H.; Polakis, P.; Junutula, J. R. Conjugation site modulates the in vivo stability and therapeutic activity of antibody-drug conjugates. *Nat. Biotechnol.* **2012**, *30*, 184.
(33) Rudé Payró, E.; Llorens Llacuna, J. Rheological characterization of the gel point in sol−gel transition. *J. Non-Cryst. Solids* **2006**, *352*, 2220−2225.
(34) Butcher, D. T.; Alliston, T.; Weaver, V. M. A tense situation: forcing tumour progression. *Nat. Rev. Cancer* **2009**, *9*, 108−122.
(35) Gucht, J.; Spruijt, E.; Lemmers, M.; Cohen Stuart, M. A. C. Polyelectrolyte complexes: Bulk phases and colloidal systems. *J. Colloid Interface Sci.* **2011**, *361*, 407−422.
(36) Luo, F.; Sun, T. L.; Nakajima, T.; Kurokawa, T.; Zhao, Y.; Sato, K.; Ihsan, A. B.; Li, X.; Guo, H.; Gong, J. P. Oppositely charged polyelectrolytes form tough, self-healing, and rebuildable hydrogels. *Adv. Mater.* **2015**, *27*, 2722−2727.
(37) Luo, F.; Sun, T. L.; Nakajima, T.; Kurokawa, T.; Ihsan, A. B.; Li, X.; Guo, H.; Gong, J. P. Free reprocessability of tough and self-healing hydrogels based on polyion complex. *ACS Macro Lett.* **2015**, *4*, 961−964.
(38) Cui, X.; Hartanto, Y.; Zhang, H. Advances in multicellular spheroids formation. *J. R. Soc., Interface* **2017**, *14*, 20160877.
(39) Manuel Iglesias, J.; Beloqui, I.; Garcia-Garcia, F.; Leis, O.; Vazquez-Martin, A.; Eguiara, A.; Cufí, S.; Pavon, A.; Menendez, J. A.; Dopazo, J.; Martin, A. G. Mammosphere formation in breast carcinoma cell lines depends upon expression of E-cadherin. *PLoS One* **2013**, *8*, No. e77281.
(40) Comşa, Ş.; Cimpean, A. M.; Raica, M. The story of MCF-7 breast cancer cell line: 40 years of experience in research. *Anticancer Res.* **2015**, *35*, 3147−3154.
(41) Albelda, S. M.; Buck, C. A. Integrins and other cell adhesion molecules. *FASEB J.* **1990**, *4*, 2868−2880.
(42) Lin, R.-Z.; Chou, L.-F.; Chien, C.-C. M.; Chang, H.-Y. Dynamic analysis of hepatoma spheroid formation: roles of E-cadherin and β1-integrin. *Cell Tissue Res.* **2006**, *324*, 411−422.
(43) Berx, G.; Van Roy, F. V. The E-cadherin/catenin complex: an important gatekeeper in breast cancer tumorigenesis and malignant progression. *Breast Cancer Res.* **2001**, *3*, 289−293.
(44) Cavallaro, U.; Christofori, G. Cell adhesion and signalling by cadherins and Ig-CAMs in cancer. *Nat. Rev. Cancer* **2004**, *4*, 118−132.
(45) Lee, B. H.; Kim, M. H.; Lee, J. H.; Seliktar, D.; Cho, N.-J.; Tan, L. P. Modulation of Huh7. 5 spheroid formation and functionality using modified PEG-based hydrogels of different stiffness. *PLoS One* **2015**, *10*, No. e0118123.
(46) Steinberg, E.; Orehov, N.; Tischenko, K.; Schwob, O.; Zamir, G.; Hubert, A.; Manevitch, Z.; Benny, O. Rapid clearing for high resolution 3D imaging of ex vivo pancreatic cancer spheroids. *Int. J. Mol. Sci.* **2020**, *21*, 7703.
(47) Yakavets, I.; Francois, A.; Benoit, A.; Merlin, J.-L.; Bezdetnaya, L.; Vogin, G. Advanced co-culture 3D breast cancer model for investigation of fibrosis induced by external stimuli: Optimization study. *Sci. Rep.* **2020**, *10*, 21273.
(48) Napolitano, A. P.; Chai, P.; Dean, D. M.; Morgan, J. R. Dynamics of the self-assembly of complex cellular aggregates on micromolded nonadhesive hydrogels. *Tissue Eng.* **2007**, *13*, 2087−2094.
(49) Whitesides, G. M.; Grzybowski, B. Self-assembly at all scales. *Science* **2002**, *295*, 2418−2421.
(50) Foty, R. A.; Steinberg, M. S. The differential adhesion hypothesis: a direct evaluation. *Dev. Biol.* **2005**, *278*, 255−263.
(51) Baker, A. E.; Tam, R. Y.; Shoichet, M. S. Independently Tuning the Biochemical and Mechanical Properties of 3D Hyaluronan-Based Hydrogels with Oxime and Diels-Alder Chemistry to Culture Breast Cancer Spheroids. *Biomacromolecules* **2017**, *18*, 4373−4384.
(52) Chang, J.; Pang, E. M.; Adebowale, K.; Wisdom, K. M.; Chaudhuri, O. Increased stiffness inhibits invadopodia formation and cell migration in 3D. *Biophys. J.* **2020**, *119*, 726−736.
(53) Ho, S. S.; Murphy, K. C.; Binder, B. Y.; Vissers, C. B.; Leach, J. K. Increased survival and function of mesenchymal stem cell spheroids entrapped in instructive alginate hydrogels. *Stem Cells Transl. Med.* **2016**, *5*, 773−781.
(54) Jiang, Q.; Pan, Y.; Cheng, Y.; Li, H.; Liu, D.; Li, H. Lunasin suppresses the migration and invasion of breast cancer cells by inhibiting matrix metalloproteinase-2/-9 via the FAK/Akt/ERK and NF-κB signaling pathways. *Oncol. Rep.* **2016**, *36*, 253−262.
(55) Huang, H.; Ding, Y.; Sun, X. S.; Nguyen, T. A. Peptide hydrogelation and cell encapsulation for 3D culture of MCF-7 breast cancer cells. *PLoS One* **2013**, *8*, No. e59482.
(56) Zolnierowicz, J.; Ambrozek-Latecka, M.; Kawiak, J.; Wasilewska, D.; Hoser, G. Monitoring cell proliferation in vitro with different cellular fluorescent dyes. *Folia Histochem. Cytobiol.* **2013**, *51*, 193−200.
(57) Khan, A. H.; Cook, J. K.; Wortmann, W. J., III; Kersker, N. D.; Rao, A.; Pojman, J. A.; Melvin, A. T. Synthesis and characterization of thiol-acrylate hydrogels using a base-catalyzed Michael addition for 3D cell culture applications. *J. Biomed. Mater. Res., Part B* **2020**, *108*, 2294−2307.
(58) Chia, J. Y.; Miki, T.; Mihara, H.; Tsutsumi, H. Biofunctional supramolecular hydrogels fabricated from a short self-assembling peptide modified with bioactive sequences for the 3D culture of breast cancer MCF-7 cells. *Bioorg. Med. Chem.* **2021**, *46*, 116345.
(59) Dumbleton, J.; Agarwal, P.; Huang, H.; Hogrebe, N.; Han, R.; Gooch, K. J.; He, X. The effect of RGD peptide on 2D and miniaturized 3D culture of HEPM cells, MSCs, and ADSCs with alginate hydrogel. *Cell. Mol. Bioeng.* **2016**, *9*, 277−288.
(60) Kudva, A. K.; Luyten, F. P.; Patterson, J. RGD-functionalized polyethylene glycol hydrogels support proliferation andin vitrochondrogenesis of human periosteum-derived cells. *J. Biomed. Mater. Res., Part A* **2018**, *106*, 33−42.

https://doi.org/10.1021/acsbiomaterials.2c01252
ACS Biomater. Sci. Eng. XXXX, XXX, XXX−XXX

(61) Joyce, M. H.; Lu, C.; James, E. R.; Hegab, R.; Allen, S. C.; Suggs, L. J.; Brock, A. Phenotypic basis for matrix stiffness-dependent chemoresistance of breast cancer cells to doxorubicin. *Front. Oncol.* **2018**, *8*, 337.
(62) Tilghman, R. W.; Cowan, C. R.; Mih, J. D.; Koryakina, Y.; Gioeli, D.; Slack-Davis, J. K.; Blackman, B. R.; Tschumperlin, D. J.; Parsons, J. T. Matrix rigidity regulates cancer cell growth and cellular phenotype. *PLoS One* **2010**, *5*, No. e12905.
(63) Burdick, J. A.; Anseth, K. S. Photoencapsulation of osteoblasts in injectable RGD-modified PEG hydrogels for bone tissue engineering. *Biomaterials* **2002**, *23*, 4315−4323.

https://doi.org/10.1021/acsbiomaterials.2c01252
ACS Biomater. Sci. Eng. XXXX, XXX, XXX−XXX